

THERMODYNAMIC ANALYSIS OF A NOVEL THERMOELECTRIC MICRO-DROPLET SENSOR

J. Ni, W. Benecke, and W. Lang

Institute for Microsensors, -Actuators and -Systems, University of Bremen, Germany

ABSTRACT

Instead of directly gauging microdrop size with expensive facilities, one can resort to a new type of droplet sensor, the design, measurement principle, and testing of which are introduced in this paper. This sensor transfers the thermopile signal induced by temperature sway in the course of droplet impinging on a regionally warmed membrane. Based on general heat conduction equation and spherically symmetric droplet-vaporization model, the enthalpy change and phase transition of concerned microdrops are explored. Derivation of essential equations is demonstrated in detail, and the mathematical tractability of such quiescent case is confirmed by experiments. The measuring method is finally suggested in the conclusion.

1. INTRODUCTION

To date there exist many strategies to measure droplet size, e.g., stroboscopic photography, electromagnetic scaling, and phase Doppler anemometry, which offer precise measurement of the geometry of droplets to the detriment of experimental effort and high cost. Maiwald [1] has reported that fallen droplets on a thermoelectric flow sensor caused the thermopile output to vary not only with the volumes of droplets but also with their thermal properties. On the basis of this observation, following theoretical analysis [2], [3], and numerical simulation [4] of droplet impingement upon a slightly heated substrate and its evaporation, a dedicated thermoelectric micro-droplet sensor has been developed at IMSAS.

Figure 1 shows the bird's-eye views of four types of fabricated sensors. In order to maximize the thermopile response during droplet collision with the heated membrane, the thermocouples are arranged in circle with a heater at the centre. These four variants of layout are achieved for the purpose of measuring volume of droplets, position of droplets, and digitizing output signal. The thermocouples are made of polysilicon and alloy tungsten-titanium. The thermopile is deposited on silicon nitride membrane ($<1 \mu\text{m}$), and covered with a passivating film of silicon nitride.

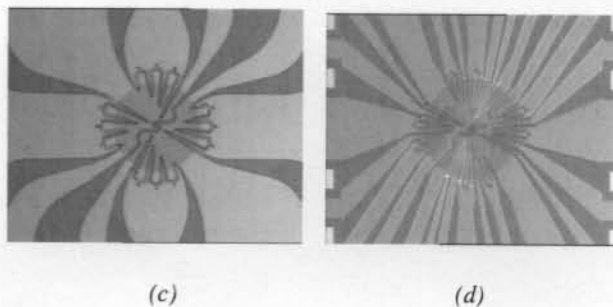
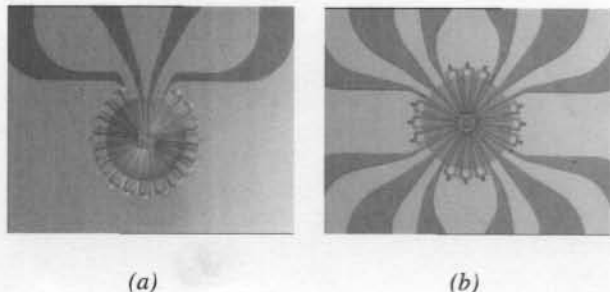


Figure 1: Four layouts of the thermoelectric droplet sensor.

2. MODELING AND TESTING

Theoretical Analysis

Various theoretical and computational aspects of fluid dynamics of droplets are comprehensively reviewed in [5], but few studies are found to address this multi-phase multi-region meniscus phenomenon. Figure 2 is a schematic of one thermoelectric sensor employed in the experiments. The precise modelling of droplet clashing on a solid surface with temperature gradient and its vaporescence entails solving Navier-Stokes equations (conservation of momentum), conservation of energy equations, mass diffusion equations, and Clausius-Clapeyron relation. They are evaluated normally by means of finite volume method. Since it necessitates much computational efforts, and makes prototyping sensors complicated, a simple model is anticipated.

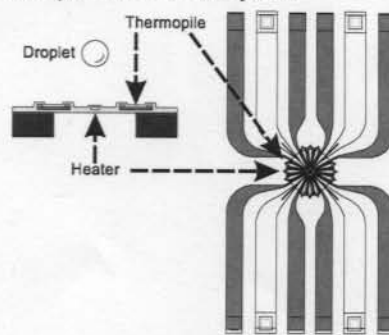


Figure 2: Schematic of one thermoelectric sensor adopted in the experiments.

Due to the low Reynolds numbers of the concerned tiny drops ($\frac{\rho_l v_l D_{drop}}{\mu} \leq 39.2$, where ρ_l is the mass density of the droplet, v_l is its velocity, D_{drop} is its diameter, and μ is its absolute dynamic fluid viscosity), deformation and advancing of droplets are assumed to occur within negligible time. The wetting area after the droplet collision with the substrate is examined through overall energy balance approach (OEB) [6].

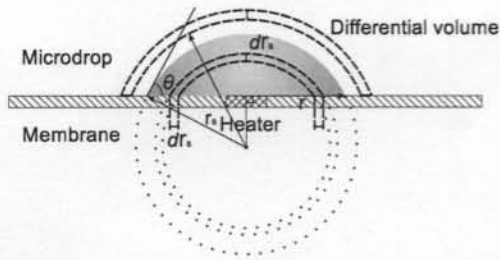


Figure 3: Cross-section of a microdroplet. The dark area shows the initial meniscus.

The meniscus is approximated as a spherical cap (Fig. 3). It is reasonable to presume that the temperature gradient inside the droplet is nearly in radial axis r_s . Cut out a spherical cap inside the meniscus with the thickness dr_s , the heat stored in the element through heat diffusion can be written as

$$F(r_s) - F(r_s + dr_s) = 2\pi r_s \left(r_s \frac{\partial^2 t_l}{\partial r_s^2} + 2 \frac{\partial t_l}{\partial r_s} \right) - 2\pi R_0 \cos \theta dr_s \left(r_s \frac{\partial^2 t_l}{\partial r_s^2} + \frac{\partial t_l}{\partial r_s} \right) \quad (1)$$

where r_s and θ are illustrated in Fig. 3, t_l is the temperature of the meniscus, λ is the thermal conductivity of the liquid, R_0 is the initial radius of the imaginary sphere, and θ is the contact angle. The heat conducted into the spherical cap from the underlying cylindrical ring with the identical thickness is reduced to $2\pi dr h_{24}(t_m - t_l)$, where r is indicated in Fig. 3, t_m is the temperature of the membrane, and h_{24} is the unit thermal conductance between the membrane and liquid. The enthalpy of the concerned spherical cap is

$$2\pi r_s (r_s - R_0 \cos \theta) \rho_l c_l \frac{\partial t_l}{\partial \beta} dr_s, \quad (2)$$

where β is time, and c_l is the specific heat capacity of the liquid. Substituting them into the extended heat conduction equation yields the conservation of energy of the spherical cap. Analogously, applying the first law of thermodynamics to the underlying cylindrical ring in the membrane, we have

$$\rho_m c_m H_m \frac{\partial t_m}{\partial \beta} = k_m H_m \nabla^2 t_m - h_{2a}(t_m - t_a) - h_{24}(t_m - t_l) \quad (3)$$

where ρ_m , c_m , k_m , and H_m are respectively the mass density, specific heat capacity, thermal conductivity, and thickness of the membrane, t_a is the ambient temperature, and h_{2a} is the heat transfer coefficient between the membrane and air. After rearrangement, we obtain the heat conduction equation for the membrane

$$\frac{\rho_m c_m}{k_m} \frac{\partial t_m}{\partial \beta} = \frac{\partial^2 t_m}{\partial r^2} + \frac{1}{r} \frac{\partial t_m}{\partial r} - \frac{h_{2a} + h_{24}}{k_m H_m} t_m + \frac{h_{24}}{k_m H_m} t_l + \frac{h_{2a}}{k_m H_m} t_a \quad (4)$$

The temperature of the heater maintains T_h , i.e.

$$t_m|_o = T_h, \quad (5)$$

where the subscript o refers to the origin. The transfer of heat near the heater is dominantly by conduction

$$-\lambda \frac{\partial t_l}{\partial r_s} \Big|_o = f_o, \quad (6)$$

where f_o is the heat flux density into the droplet at the origin. Natural convection takes place at the surface of the meniscus

$$-h_{2a} \frac{\partial t_l}{\partial r_s} \Big|_b = f'_{db}, \quad (7)$$

where f'_{db} is the gradient of the heat flux density at the meniscus surface, with the subscripts d and b respectively representing droplet and boundary. The heat flux density of the membrane under the boundary of the liquid splat f_{mb} remains constant

$$-k_m \frac{\partial t_m}{\partial r} \Big|_b = f_{mb}, \quad (8)$$

where the subscript m implies membrane. Prior to droplets striking, the temperature distribution along the membrane is the solution to the following ordinary differential equation

$$\frac{d^2 t_m}{dr^2} + \frac{1}{r} \frac{dt_m}{dr} - \frac{h_{2a}}{k_m H_m} t_m + \frac{h_{2a}}{k_m H_m} t_a = 0, \quad (9)$$

that is,

$$C_1 J_0(\sqrt{br}) + C_2 Y_0(\sqrt{br}) + t_a, \quad (10)$$

where C_1 and C_2 are the constants determined by means of boundary conditions, J_0 and Y_0 are Bessel functions, and $b = \frac{h_{2a}}{k_m H_m}$. Unifying coordinates in r , and numerically

solving the system of parabolic PDEs along with the boundary conditions and initial conditions provides the temperature change of both meniscus and the membrane under the liquid. Figure 4 delineates the temporal variations in the membrane and along the radial axis of the fallen droplet.

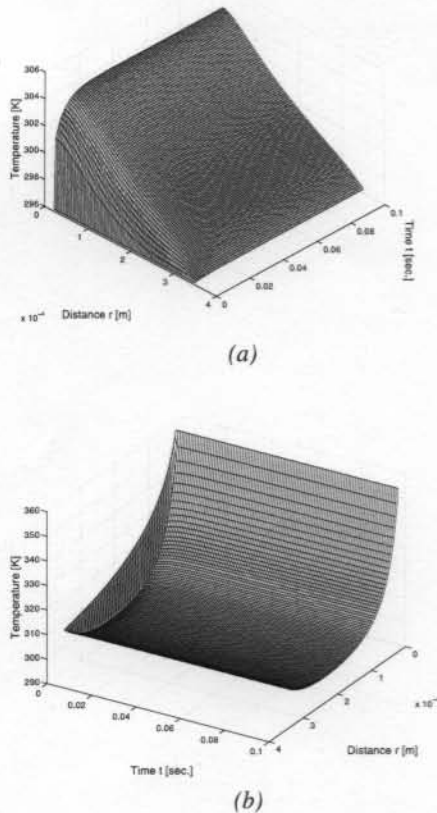


Figure 4: (a) Temperature variation of the membrane under the meniscus during impingement; (b) Temperature variation of the splat during impingement.

The thermal conductance between the membrane and the liquid is proven to have significant influence on the temperature profile of droplets at quasi thermal equilibrium. In case of large thermal conductance, the temperature profiles of the membrane and droplet overlapped each other for the large distance from the origin. The temperature distribution of the meniscus is substantially linear in terms of small thermal conductance. Both of them lead to further simplification of the relation between the droplet volume and the sensor output.

In order to investigate the evaporation of the liquid splat, a differential volume in the vapour above the meniscus is chosen as shown in Fig. 3. The upper surface area for the spherical cap is $A(r_s)$. The energy balance inside the differential element is

$$A(r_s)\rho v c_p \frac{dt}{dr_s} = \lambda_v \frac{d}{dr_s} \left(A(r_s) \frac{dt}{dr_s} \right), \quad (11)$$

where t is the temperature of the volume under consideration, ρ is the vapour mass density, v is the diffusion velocity, c_p the thermal capacity of the vapour mixture, and λ_v is the thermal conductivity of the mixture.

The boundary condition at the surface of the meniscus is

$$-\lambda_v \left. \frac{dt}{dr_s} \right|_b = \rho_b v_b L, \quad (12)$$

where ρ_b is the vapour mass density at the surface of the liquid splat, v_b is the diffusion velocity at the surface, and L is the latent heat of vaporization. Solving (11) yields

$$\frac{A(r_{sb})\rho_b v_b c_p}{2\pi\lambda_v R_0 \cos\theta} \ln \frac{r_s - R_0 \cos\theta}{r_s} = \ln \frac{t - t_b + \frac{L}{c_p}}{t_\infty - t_b + \frac{L}{c_p}}, \quad (13)$$

where t_∞ is the ambient temperature surrounding the meniscus. From (13) $\rho_b v_b$ is determined as $t = t_b$, which is the outcome of (1) and (4). Reference [3] has shown that the evaporation can be better modelled as portion of a dwindling spheroid with fixed spherical centre, and the evaporation rate of the meniscus for quasi-steady case can be equivalently expressed by

$$\rho_b v_b = -\rho_l \frac{dr_b}{d\beta}. \quad (14)$$

Substituting $\rho_b v_b$ in (14), we finally come to the formula calculating the shrinking radius of the wetting area

$$r_{new} = r + \frac{dr}{d\beta} \delta\beta. \quad (15)$$

Based on (15), the evaporation process of the liquid splat is modelled in reiteration, namely, the temperature of the meniscus and membrane, and the evaporation rate are successively calculated over the course of phase transition.

Verification and General Testing of Sensors

In an attempt to validate this model, an experimental setup has been established. The peripherals to the sensor circuit mainly include a constant voltage source for driving the heater as well as the signal acquisition to sample and convert the signals from the thermopile. After conditioning and communicating through a serial port, the data is saved on a PC. In order to avoid strong coupling between the liquid and gas phases, the voltage to the heater is maintained at 1.5 V, which corresponds to 356.6 K according to VarioTHERM™, a real-time thermographic system from Infratec. The droplets were generated with a Piezodropper™ from IWT. The droplet size is dependent on the magnitude, width, and the frequency of the driving impulse on the piezoelectric nozzle. For calibration, an optical system was added. Part of the experimental configuration is illustrated in Figure 5. Figure 6 displays the comparison between the aforementioned model with the reality which is the output signal of the thermopile in layout 1. The deviation in the initial phase is essentially due to ignorance of thermal convection inside the meniscus and geometric alteration of the droplet. The assumption on droplet

shape and the nonlinear Seebeck coefficient lead to the discrepancy in the evaporation stage.

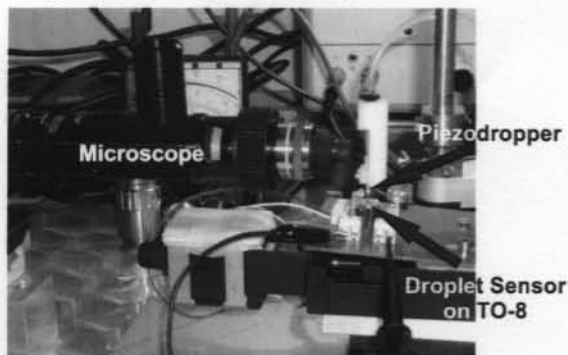


Figure 5: Test stand for the droplet sensor with layout 1.

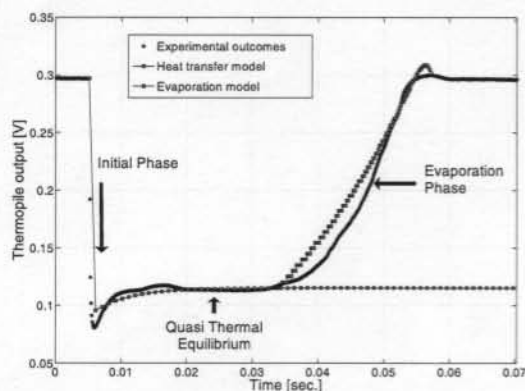


Figure 6: Model validation for microdroplet $\text{Ø}43.0 \mu\text{m}$. Experimental data in dotted blue line; Prediction in dark boxed line.

Four types of such sensors were measured. Sensors with layout 1 offered the highest output voltage up to 1.0 V at 3 V driving tension. Chips with layout 2 provided the possibility to measure the position of the fallen droplet with resolution of $10 \mu\text{m}$. Stepwise signals were generated from sensors with layout 3. Sensors with layout 4 produced a kind of combination of the layout 2 and layout 3, but indicated the lowest signal. Sample output signals are displayed in Fig. 7, where Figure 7 (a) gives the information on the location of the microdrop, four levels can be extracted from the curve in Fig. 7 (b).

3. CONCLUSIONS

This work discusses an innovative droplet sensor. Its theoretical analysis is affirmed with final experimental results. Some typical outputs of these sensors are presented. Equation (13) reveals that the evaporation rate is correlated with the size as well as the contact angle of the meniscus, which relates to the surface material and process condition. It appears that these sensors are more suitable for theoretically detecting microdrop size by

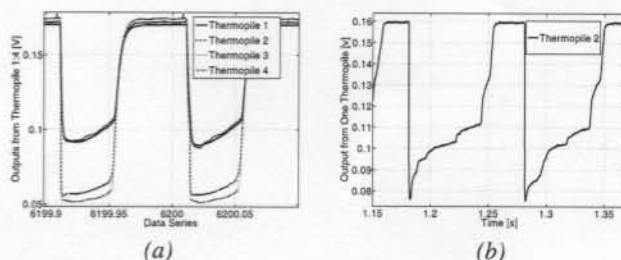


Figure 7: (a) Thermopile outputs of the sensor with layout 2; (b) Thermopile output of the sensor with layout 3.

virtue of the proven model. Some key parameters, e.g., surface tension of the passivating layer, k_m , and h_{2a} , are expected to be investigated beforehand. Alternatively, a database containing the steady voltages at quasi thermal equilibrium with respect to diverse heating power and droplet sizes can be experimentally built. Both of them require a processor for curve fitting. In addition to determining droplet volume, sensors with layout 2, 3, and 4 possess the capability of detecting the fallen position of microdrops.

Further study will focus on high-order relation between the evaporation rate and the liquid properties, and realizing of the signal-processing circuit, which could be prototyped on platform Matlab/xPC Target.

ACKNOWLEDGMENT

We are very grateful to Dr.-Ing. Thomas Wriedt and Dipl.-Ing. Norber Riefler for their worthwhile advice and use of the piezoelectric droplet generator, which plays a key role at our current experiments.

REFERENCES

- [1] M. Maiwald, R. Buchner, J. Ni, V. Zöllmer, I. Wirth, M. Busse, W. Benecke, and W. Lang, "Droplet characterisation using thermoelectric sensors," Proc. of 20th Eurosensors, W2C-O2, September 2006.
- [2] J. Ni, M. Maiwald, R. Buchner, C. Sosna, W. Benecke, and W. Lang, "Simple modelling of the thermal behaviour of a tiny liquid splat on a thermal microsensors," Journal of Microelectromechanical Systems, vol. II, pp. 473-479, April 2007.
- [3] J. Ni, W. Benecke, and W. Lang, "Evaporation model of micro-menisci for thermoelectric drop sensor," IEEE Sensors 2007, (in press).
- [4] J. Ni, W. Benecke, and W. Lang, "Multiphysics analysis of deformation and phase transition of a heated droplet," Proc. of Smart Systems Integration 2007, pp.569-572, March 2007.
- [5] W. A. Sirignano, *Fluid dynamics and transport of droplets and sprays*, Cambridge University Press, USA, 1999.
- [6] D. Erickson, B. Blackmore and D. Li, "An energy balance approach to modeling the hydrodynamically driven spreading of a liquid drop," Colloids and Surfaces, A 182, pp. 109-122, 2001. Trans. on Comp. and Pack. Tech., vol. 26, no. 1, pp. 215-221, March 2003.